Surface photovoltage spectroscopy of metamorphic high electron mobility transistor structures

S. Solodky and T. Baksht
School of Electrical Engineering, Tel-Aviv University, Ramat-Aviv 69978, Israel

A. Khramtsov
Department of Electrical and Computer Engineering, Ben-Gurion University, Beer-Sheva 84105, Israel

M. Leibovitch
Gal-El (MMIC), P.O.B. 330, Ashdod 77102, Israel

S. Hava
Department of Electrical and Computer Engineering, Ben-Gurion University, Beer-Sheva 84105, Israel

Yoram Shapira[a)]
School of Electrical Engineering, Tel-Aviv University, Ramat-Aviv 69978, Israel

(Received 30 March 2004; accepted 5 July 2004; published 13 October 2004)

InAlAs/InGaAs metamorphic high electron mobility transistor (MHEMT) epitaxial structures have been characterized using surface photovoltage spectroscopy (SPS). The measurements have been extended to pseudomorphic high electron mobility transistor (PHEMT) epitaxial structures and to complete devices. The direct current characteristics of the latter were also measured. An empirical model, which correlates the top and bottom delta-doping concentrations (δ_{top} and δ_{bot}) and the surface charge density Q_{sur} with spectral features, has been applied to the MHEMT and PHEMT structures before and after processing. The results show correlations between extracted Q_{sur} and the measured threshold voltage and drain saturation current of the devices. The analysis shows general correlations between epistructure parameters and final device performance and indicates the universality of the model for the different HEMT structures. Thus, SPS is sensitive not only to epitaxial structure parameters but to final device performance and may be used for technology evaluation from the wafer incoming inspection stage to the final device. © *2004 American Vacuum Society.* [DOI: 10.1116/1.1787518]

I. INTRODUCTION

Metamorphic high electron mobility transistors (MHEMTs) are attractive for low noise, high speed applications due to their high cutoff and maximum oscillation frequencies[1,2] as well as their low cost GaAs substrates. MHEMTs are preferable over the widely used pseudomorphic HEMTs (PHEMTs) because of the higher In concentrations in their InGaAs channels and also thicker channels, although MHEMTs suffer from higher defect densities due to the metamorphic growth process.

The complex design and growth procedures of MHEMTs require an effective characterization technique for monitoring growth quality and device parameters as early as possible before and after processing. The measurement technique should be contactless, nondestructive, fast, and wafer-scaled. Indeed, photoluminescence [3,4] and x-ray diffraction[5] have been used for the characterization of MHEMT structures.

Surface photovoltage spectroscopy (SPS) is a method, which fulfills most of the demands for comprehensive transistor structure characterization and for incoming wafer inspection.[6] SPS monitors changes in the semiconductor surface work function induced by absorption of monochromatic light, giving rise to surface photovoltage (SPV). A detailed description of this method and its applications may be found in Ref. 7. This technique has been successfully applied for characterization of structures and devices.[8–12]

In this work, MHEMT structures have been characterized using SPS measurements and numerical simulations. We introduce an empirical model, which correlates spectral features and epitaxial structure parameters. Applying the empirical model to MHEMT and PHEMT structure analysis shows the universality of the model for different HEMT structures. We show examples of the model application to comparison of MHEMT epitaxial structures before and after processing. Direct current (dc) measurements performed on complete devices show correlations between epistructure parameters and final device performance.

II. EXPERIMENT

A double-sided delta doped MHEMT structure grown by molecular beam epitaxy on a GaAs substrate is shown in Fig. 1. It consists of several layers: (1) A metamorphic InAlAs buffer with graded In composition and a typical thickness about 1 μm. The purpose of the metamorphic buffer is to match between the GaAs and InGaAs lattice constants. (2) InAlAs (with a typical In composition of 50% and a thickness of 35–45 nm) buffer. The purpose of the InAlAs buffer is to prevent metamorphic buffer defects from reaching the active region of the device. (3) Two delta-doped layers of

[a)]Electronic mail: Shapira@eng.tau.ac.il

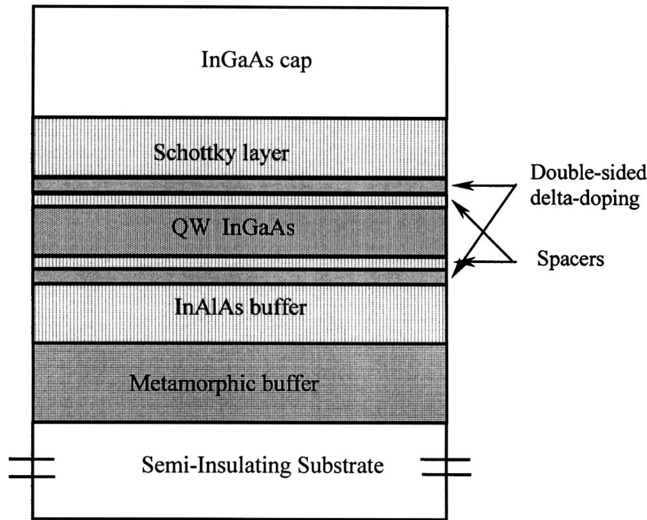

FIG. 1. Typical epitaxial structure of a MHEMT.

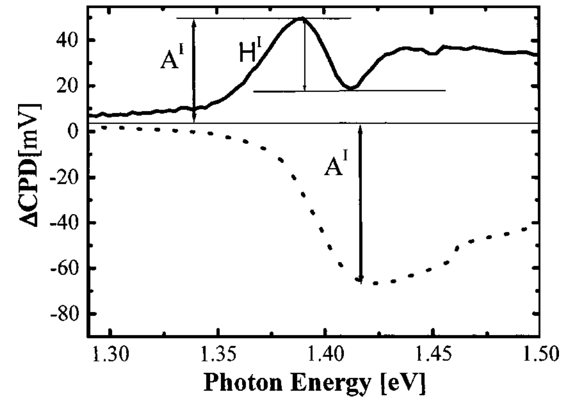

FIG. 2. Experimental CPD spectra of a PHEMT (solid curve) and a MHEMT (circles). Labels correspond to the spectrum parameterization scheme: A^I—first peak amplitude, H^I—first peak height.

n^+-InAlAs (with Si sheet concentration in the range of $1-6 \times 10^{12}$ cm^{-2}) on both sides of the channel, which are the source of electrons for the conductive channel. (4) Two layers 4–5 nm thick of undoped InAlAs, acting as spacers that separate the donors further from the channel electrons and reduce Coulomb scattering. (5) An undoped InGaAs quantum well (QW) (with a typical In mole fraction of ~50%) provides the conductive channel, in which the electrons are strongly confined. (6) An undoped 10–15 nm InAlAs layer (also known as the Schottky layer), on top of the InAlAs delta-doped layer, separates the channel from the gate electrode. (7) The structure top layer is a highly doped n^+-InGaAs cap, which is used for source and drain Ohmic contact formation.

The SPS measurements were performed in air using a commercial Kelvin probe unit (Besocke Delta Phi, Julich, Germany). The optical system consists of a 250 W tungsten–halogen lamp, a double monochromator (McPherson, USA) and a set of bandpass filters to avoid second order harmonics. The measurement sensitivity is about 1 mV and the light intensity is in the order of 10 μW/cm^2 at a wavelength of 750 nm. Neutral density filters control the light intensity. In SPS, the change in the contact potential difference (CPD) between a gold Kelvin probe and a semiconductor surface as a result of illumination is monitored. The CPD is defined as

$$e\text{CPD} = W_s - W_m, \quad (1)$$

where W_s is the semiconductor surface work function and W_m is the Kelvin probe work function. Since the work function of the metallic electrode does not change under illumination, one can assume that the difference between the CPD under illumination and the dark CPD is given by

$$e \cdot \Delta\text{CPD} = \Delta W_s = -e \cdot \Delta V_s = -e \cdot \text{SPV}, \quad (2)$$

where V_s is the surface potential. The ΔCPD that is monitored by the Kelvin probe method is opposite in sign to the SPV. The SPV spectra analysis is based on quantitative numerical modeling. The Poisson equation, the continuity equations for electrons and holes, and the current equations are numerically solved.[13] The initial conditions for the numerical model can be obtained from the equilibrium distributions of electrons and holes and the electrostatic potential obtained by the procedure outlined in Ref. 14. Various semiconductor interfaces, based on different materials, are present within the device. Therefore, all the structural parameters, including electron affinity (work function) and mobility are considered as position dependent.

The system of the relevant partial differential semiconductor equations, together with appropriate boundary and initial conditions, cannot in general be solved explicitly. Therefore, the solution is obtained numerically. For the specific problem in this work, we have used the finite difference method described elsewhere.[15] It has been successfully used for the characterization of different structures and devices. The detailed description of these applications is outlined in Refs. 8–11.

Self-aligned-gate MHEMT devices have been fabricated with 0.25 μm Ti/Pt/Au and Ti/Pt gates. A description of the self-aligned gate MHEMT fabrication may be found in Refs. 16 and 17. The source-drain Ohmic contacts were made using Ni\Au\Ge\Au metallurgy. All dc measurements were performed on a HP 4551B semiconductor analyzer.

III. EMPIRICAL MODEL

Figure 2 shows parts of CPD experimental spectra of double-sided PHEMT (solid curve) and MHEMT (circles) structures. At the low energy region, absorption takes place in the QW. At this portion of the spectrum, the PHEMT signal increases while the MHEMT signal decreases. At photon energies above 1.4 eV, a second peak in the PHEMT spectrum is observed. This feature may be attributed to absorption in GaAs. At low photon energies, Fermi filling, due to high electron concentration in the channel, dominates the InGaAs absorption.[18] This effect significantly changes the absorption coefficient of the QW by blueshifting its edge and reducing its magnitude at higher energies.

Typical HEMT structures are designed in such a way that there are two oppositely directed electric fields in the buffer

and in the Schottky layer.[19] Thus, the SPV signals from these layers are of opposite signs. Numerical simulations performed for PHEMT structures show that the total SPV signal is a combination of the signals from all structure layers. Absorption of light in the QW creates electron-hole pairs. While electrons are confined within the QW by fields in the buffer and Schottky layers, holes are likely to overcome the QW-Schottky layer interface or the QW-buffer interface potential barrier. The holes are swept by the electric field in the buffer or in the Schottky layer, contributing to signals with opposite signs—a positive signal from the buffer and a negative one from the Schottky layer. This makes it possible to decode the spectrum in the QW region according to the signal sign.

Figure 2 shows parts of CPD spectra in the QW region of absorption of the PHEMT and MHEMT structures. The light absorption occurs in the QW. In the case of the PHEMT spectrum, a positive signal is observed at lower energies. This is because the dominant signal comes from the buffer. When the signal from the buffer is saturated, the total SPV changes sign because of the dominating signal from the Schottky layer. The start of absorption in the GaAs buffer is the reason for the signal increase at a photon energy of 1.41 eV and the second peak formation in the PHEMT spectrum. In the case of the MHEMT SPV spectrum, a negative signal is observed in QW region of absorption. This is because the dominant signal comes from the Schottky layer region. The signal sign changes when the Schottky layer contribution is saturated. The second peak related to GaAs absorption does not appear in the MHEMT spectrum because there is no GaAs buffer in that structure. The energy of the first peak appearance is dictated by the electric field distribution within the structure while this energy position is a result of signal saturation from one of the layers (Schottky or buffer). This saturation is a result of a reduced electric field in the layer due to photogenerated charge redistribution. Thus, the higher the initial electric field in the layer, the higher is the photon energy where saturation occurs (if at all). Therefore, the spectral shape in the QW region of absorption is defined by the electric field distribution within the structure. The different charge densities in the structure may cause spectra shape changes. We developed an empirical model that correlates the SPV spectrum and the HEMT structural parameters.

The spectra of the HEMT structures were parameterized in Fig. 2. The spectral parameters are the amplitude of the first peak (or minimum)—A^I and the peak height (relative to the interpeak valley)—H^I. The signal amplitude is defined by the overall electric fields distribution in the structure, which is dictated by the top and bottom delta-doping levels δ_{top} and δ_{bot} and surface charge density Q_{sur}. Thus, A^I depends on all charge densities in the structure. H^I is a result of the strong interplay between the signals from the Schottky and buffer layers. This interplay depends on the electric field distribution in the buffer and Schottky layers, which is defined by δ_{top} and δ_{bot}.

An empirical model, which correlates the spectral features (A^I,H^I) and the structural parameters (δ_{top}, δ_{bot}, and Q_{sur}) has been developed using numerical simulations. This model has been applied to several PHEMT structures. The efficacy of the model for PHEMT characterization is shown in Ref. 12. δ_{top}, δ_{bot}, and Q_{sur} are changed in the simulated structures and their effects on A^I and H^I in simulated spectra are analyzed. A two-level factorial design[12,20,21] has been used to define the device structure with different combinations of structural parameters. Detailed description of the modeling procedure and the model coefficients is given in Ref. 12. The model shows that the differences in the spectral parameter A^J (relative to a reference structure) are given by

$$\Delta A^J(\delta_{\mathrm{top}},\delta_{\mathrm{bot}},Q_{\mathrm{sur}}) = C_{\delta\mathrm{top}}\Delta\delta_{\mathrm{top}} + C_{\delta\mathrm{bot}}\Delta\delta_{\mathrm{bot}} + C_{Q_{\mathrm{sur}}}\Delta Q_{\mathrm{sur}}, \tag{3}$$

where $C_{\delta\mathrm{top}}$, $C_{\delta\mathrm{bot}}$, $C_{Q_{\mathrm{sur}}}$ are coefficients, which weight the influence of each of the electrical parameters on the spectral parameter A^J.

The spectra of a double-sided delta-doped PHEMT (represented by the solid curve in Fig. 2) and a MHEMT (circles) have been compared. The δ_{top} in the PHEMT structure is 5.45×10^{12} cm^{-2}. The structures have the same δ_{bot} level while the difference in δ_{top} specified by the supplier is 1×10^{12} cm^{-2}. Variations in δ_{top} change the electric field distribution in the Schottky layer region and thus the spectral shapes of the QW absorption region significantly differ. The difference in δ_{top} between PHEMT and MHEMT structures has been calculated using the model. Q_{sur} is assumed to be the same, which reduces Eq. (3) to $\Delta A^I=130\Delta\delta_{\mathrm{top}}$. The calculated $\Delta\delta_{\mathrm{top}}$ is 0.9×10^{12} cm^{-2}, which is in good agreement with the grower specifications.

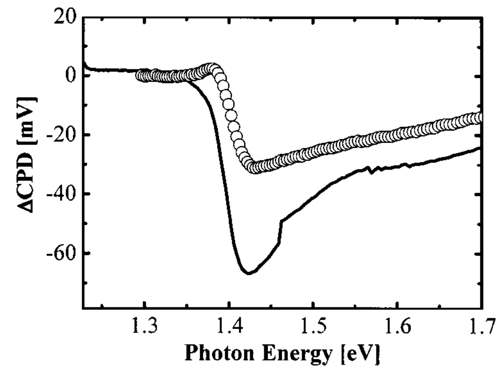

FIG. 3. Experimental CPD spectra of two MHEMT structures: *M*1 (solid curve) and *M*2 (circles).

IV. MHEMT RESULTS

Figure 3 shows experimental CPD spectra of two MHEMT structures: *M*1 (solid curve) and *M*2 (circles). There is a difference in the δ_{top} level between the two structures, denoted by $\Delta\delta_{\mathrm{top}}$. A higher δ_{top} in *M*2 leads to the dominating signal from its buffer layer and an overall positive signal in the QW region. The δ_{top} of *M*1 is $4.45\times10^{12}\pm0.45\times10^{12}$ cm^{-2}. The $\Delta\delta_{\mathrm{top}}$ extracted from the

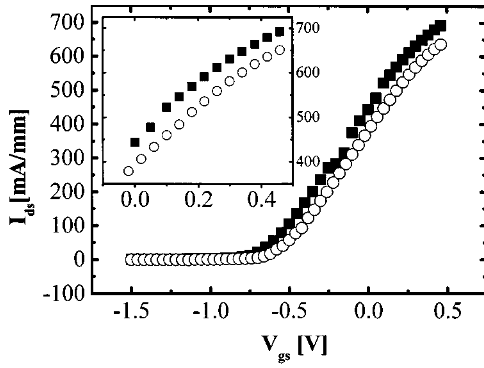

FIG. 4. $I_{ds}(V_{gs})$ curves of 100 μm gate periphery transistors produced on epistructures $M1$ (circles) and $M2$ (squares) structures. Inset shows part of $I_{ds}(V_{gs})$ curves at positive V_{gs} and indicates differences in I_{max}.

model is $0.50\times10^{12}\pm0.05\times10^{12}$ cm^{-2}, which is in good agreement with the grower specification $-0.55\times10^{12}\pm0.05\times10^{12}$ cm^{-2}.

In order to check the robustness of the model in wafer incoming inspection, 0.25 μm devices have been fabricated on wafers with epistructures similar to $M1$ and $M2$ structures. The device characteristics related directly to the delta-doping level is the maximum drain-source current—I_{max}. I_{max} is defined as the drain current at maximum gate voltage. This current is given by the expression

$$I_{max}=qn_S\nu_S w, \quad (4)$$

where q is the electron charge, n_s is the channel electron sheet density, ν_s is the electron saturation velocity in the channel, and w is the gate periphery, which is defined as a gate finger width times the number of gate fingers. For devices with the same gate periphery (w), I_{max} is defined by n_S, which is given by

$$n_s=\int_{x1}^{x2} n(x)dx, \quad (5)$$

where $n(x)$ is the distribution of mobile charges within the well, x_1 and x_2 are the coordinates of the buffer/QW and the QW/Schottky layer interfaces, respectively.[22] $n(x)$ is directly related to the delta-doping levels.

The $I_{ds}(V_{gs})$ curve of two-finger transistors with 100 μm gate periphery manufactured on two wafers has been measured, where I_{ds} is the drain-source current and V_{gs} is the gate-source voltage. Figure 4 shows $I_{ds}(V_{gs})$ curves for transistors with 100 μm gate periphery fabricated on $M1$ (circles) and $M2$ (squares) structures measured at a drain-source voltage of $V_{ds}=1$ V. The inset shows part of the $I_{ds}(V_{gs})$ for positive V_{gs} voltages. Table I summarizes the results of comparing the two epistructures and fabricated devices. The results show a good correlation between supplier data, differences in δ_{top} extracted from the model and final device performance. This demonstrates the sensitivity of the methodology to even slight differences in the delta-doping level. The model enables prediction of the device dc and power performance.

TABLE I. Results of SPS and dc characterization of two MHEMT structures.

δ_{top} for MHEMT structure $M1$ (cm^{-2})	4.45×10^{12}
Relative $\Delta\delta_{top}$ by supplier (%)	12
Relative $\Delta\delta_{top}$ from model (%)	11
Relative ΔI_{max} calculated (%)	12

V. SPS ON MHEMT DEVICES

Figure 5 shows the QW absorption parts of CPD spectra of two wafers with fabricated MHEMT devices, $W1$ (solid line) and $W2$ (circles). The two wafers had the same epitaxial structure before the fabrication process with $\delta_{top}=5\times10^{12}$ cm^{-2}. The process steps included conventional alloyed Ohmic contacts and a self-aligned submicron T gate. The minimum signal magnitude at $E=1.43$ eV differs by 28 mV. This difference may be related to differences in Q_{sur} between the two wafers—ΔQ_{sur}. Q_{sur} extracted from the model for $W2$ is 1.3×10^{13} cm^{-2}. Applying the model for comparing the two spectra yielded ΔQ_{sur} showing a more positive surface charge density at $W1$ by 5.6×10^{12} cm^{-2}, i.e., an increase of 40% in Q_{sur}. The device threshold voltage V_T is proportional to the doping density.[22] A more positive surface charge density means an additional positive potential at the surface. It changes the potential profile of the structure in such a way that the Fermi level is at a higher energy position within the channel. In this case, without any applied V_{gs}, the channel is less depleted and the electron sheet density in the channel is higher. Thus, more negative V_{gs} should be applied to deplete electrons from the channel. Such a structure requires a more negative threshold voltage V_T and a higher drain current at $V_{gs}=0$, I_{dss} to operate. To obtain a correlation between the surface charge density, extracted from the SPS measurements, and device performance, identical coplanar devices with 200 μm gate periphery on $W1$ and $W2$ have been characterized and compared. Results of the device comparison on $W1$ and $W2$ are given in Table II. The results show for $W1$ I_{dss}, and the absolute value of V_T are higher by about 20% relative to $W2$.

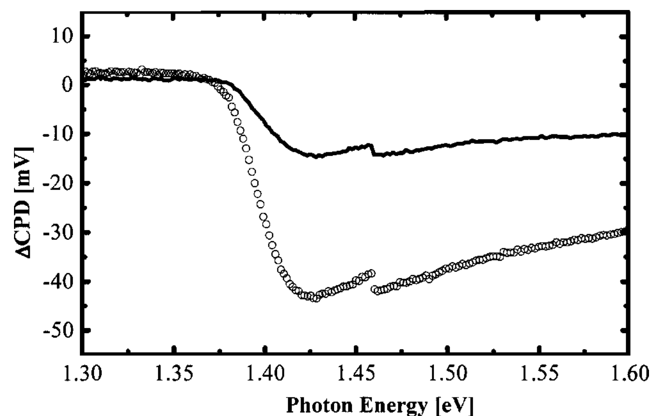

FIG. 5. QW absorption parts of CPD spectra from two wafers with fabricated devices, $W1$ (solid curve) and $W2$ (circles).

TABLE II. Results of dc characterization of devices produced on $W1$ and $W2$.

	I_{dss} (mA/mm)	V_T (V)
$W1$	304	−0.87
$W2$	258	−0.72

VI. CONCLUSIONS

A methodology of MHEMT technology characterization, using SPS has been developed. The methodology is used for technology evaluation from the wafer incoming inspection stage to the final device stage. A universal empirical model developed for PHEMT structures has been tested on MHEMT structures and successfully applied for comparing PHEMT and MHEMT structures. Based on the model, the differences of doping density between different MHEMT structures have been found. These differences correlate with characterization results of final devices fabricated on two structures: a relative difference of 12% in I_{max} correlates with a relative difference of 11% in δ_{top} extracted from SPS characterization of the structures before processing. In addition, SPS measurements have been performed on two structures after processing. Differences in surface charge density have been found from SPV spectra. The results of SPS characterization correlate with the results of dc characterization of the fabricated devices. Devices with increased positive surface charge density shows increased I_{dss} and absolute value of V_T.

[1]Y. Yamashita, A. Endoh, K. Shinohara, M. Higashiwaki, K. Hikosaka, T. Mimura, S. Hiyamizu, and T. Matsui, IEEE Electron Device Lett. **22**, 367 (2001).
[2]S. Bollaert, Y. Cordier, M. Zaknoune, T. Parenty, H. Happy, S. Lepilliet, and A. Cappy, Electron. Lett. **38**, 389 (2002).
[3]M. Wojtowicz, D. Pascua, A. C. Han, T. R. Block, and D. C. Streit, J. Cryst. Growth **175**, 930 (1997).
[4]W. Lu, J. H. Lee, K. Prasad, G.-I. Ng, and P. Lindstrom, J. Phys. D **31**, 159 (1998).
[5]T. J. Rogers, J. M. Ballingall, M. Larsen, and E. L. Hall, J. Vac. Sci. Technol. B **13**, 777 (1995).
[6]Y. T. Cheng, Y. Huang, D. Y. Lin, F. H. Pollak, and K. R. Evans, Physica E (Amsterdam) **14**, 313 (2002).
[7]L. Kronik and Y. Shapira, Surf. Interface Anal. **31**, 954 (2001).
[8]B. Mishori, M. Leibovitch, Y. Shapira, F. H. Pollak, D. C. Streit, and M. Wojtowicz, Appl. Phys. Lett. **73**, 650 (1998).
[9]N. Bachrach-Ashkenasy, L. Kronik, Y. Shapira, Y. Rosenwaks, M. C. Hanna, M. Leibovitch, and P. Ram, Appl. Phys. Lett. **68**, 879 (1996).
[10]N. Ashkenasy, M. Leibovitch, Y. Shapira, F. H. Pollak, T. Burnham, and X. Wang, J. Appl. Phys. **83**, 1146 (1998).
[11]N. Ashkenasy, M. Leibovitch, Y. Rosenwaks, Y. Shapira, K. W. J. Barnham, J. Nelson, and J. Barnes, J. Appl. Phys. **86**, 6902 (1999).
[12]S. Solodky, N. Ashkenasy, M. Leibovitch, I. Hallakoun, Y. Rosenwaks, and Y. Shapira, J. Appl. Phys. **88**, 6775 (2000).
[13]G. A. Ashkinasi, M. G. Leibovitch, and M. Nathan, IEEE Trans. Electron Devices **40**, 285 (1993).
[14]A. Marshak, Solid-State Electron. **24**, 1111 (1981).
[15]S. Selberherr, *Analysis and Simulation of Semiconductor Devices* (Springer, New York, 1984).
[16]M. Kao, E. A. Beam III, T. Yun, C. F. Campbell, M. S. Heins, P. Saunier, J. B. Delaney, and R. A. Eye, International Conference on Indium Phosphide and Related Materials, 2003, p. 361 (unpublished).
[17]M. Zaknoune, B. Bonte, C. Gaquiere, Y. Cordier, Y. Druelle, D. Theron, and Y. Crosnier, IEEE Electron Device Lett. **19**, 345 (1998).
[18]Y. H. Zhang and K. Ploog, Phys. Rev. B **45**, 14069 (1992).
[19]W. E. Quinn, B. Lauterwasser, J. Kronwasser, T. Mizandi, and D. Carlson, 1997 International Conference of GaAs Manufacturing Technology (MANTECH) Digest, p. 166.
[20]H. G. Henry and K. M. Renaldo, 1998 International Conference of GaAs Manufacturing Technology (MANTECH) Digest, p. 195.
[21]G. E. P. Box, W. J. Hunter, and J. S. Hunter, *Statistics for Experiments* (Wiley, New York, 1978).
[22]L. D. Ngyen, L. E. Larson, and U. K. Mishra, Proc. IEEE **80**, 494 (1992).